# Improvements in the regional earthquake focal mechanism catalogue for southwestern Yukon

Jeremy M. Gosselin*, Katherine Biegel, Mahdi Hamidbeygi and Jan Dettmer
Department of Geoscience, University of Calgary

Gosselin, J.M, Biegel, K, Hamidbeygi, M. and Dettmer, J., 2023. Improvements in the regional earthquake focal mechanism catalogue for southwestern Yukon. *In:* Yukon Exploration and Geology 2022, K.E. MacFarlane (ed.), Yukon Geological Survey, p. 63–76 plus digital appendices.

## Abstract

Earthquake source characteristics provide a valuable constraint on fault behaviour, crustal stress, and regional plate tectonics. In southwestern Yukon, a region of complex active tectonics, studies of earthquake sources have historically been limited by sparse seismic network coverage. In this work, we leverage recent improvements in station coverage to estimate focal mechanisms for small and moderate-magnitude ($M \geq 2.0$) earthquakes from P-wave first-motion polarity data. We invert these data using a probabilistic method that rigorously quantifies mechanism uncertainties. We present preliminary solutions for 363 events, which improve the spatial coverage of the focal mechanism catalogue for this region. We observe contrasting P-axis orientations for events on either side of the Fairweather fault. For events within southwestern Yukon, the distribution of faulting mechanism types and P-axis orientations are relatively consistent. Our focal mechanism solutions support the existence of an unmapped fault south of the Duke River fault. Finally, our results provide a valuable input for subsequent detailed analysis of crustal stress throughout the region.

* jeremy.gosselin@ucalgary.ca

# Introduction

## Tectonic setting

Southwestern Yukon is a region of complex active tectonics, where strike-slip motion along the Queen Charlotte-Fairweather fault system transitions to oblique convergence of the Pacific plate (and Yakutat block/microplate) with the North American plate (Leonard *et al.*, 2007). This convergence is partitioned between the Aleutian trench subduction system and a series of right-lateral crustal strike-slip fault systems (Fig. 1), with oblique convergence of the Pacific plate (relative to North America) occurring at a rate of approximately 57 mm/yr (Kreemer *et al.*, 2014). In southeastern Alaska and Yukon, plate motion is accommodated by deformation along the Denali fault and associated nearby fault systems, including thrusting and uplift of the St. Elias Mountains.

The arcuate Denali fault system extends over 2000 km from British Columbia, through Yukon and central Alaska, and ultimately to the Bering Sea (Fig. 1 inset). The Denali fault represents a geological boundary between the accreted Insular and Intermontane terranes of the North American Cordillera (Nelson *et al.*, 2013), and has experienced total right-lateral displacement of approximately 400 to 480 km (Lowey, 1998; Waldien *et al.*, 2021). Topography, geodetic constraints, and Quaternary fault mapping suggest that the Central Denali fault (also called the McKinley segment; through central Alaska) is more tectonically active compared to the Eastern Denali fault that extends through Yukon (*e.g.*, Haeussler *et al.*, 2008; Bemis *et al.*, 2015; Marechal *et al.*, 2015, 2018). The Eastern Denali fault includes the Shakwak segment that intersects the Totschunda fault, as well as the southernmost Dalton segment that extends southward to the Chatham Strait (Grantz, 1966). Slip rates along the Denali fault are estimated to decrease eastward from approximately 12 mm/yr along the central section, to 5–8.4 mm/yr along the Shakwak segment, and 1–2.5 mm/yr along the Dalton segment (*e.g.*, Matmon *et al.*, 2006; Leonard *et al.*, 2007, 2008; Kalbas *et al.*, 2008; Elliott *et al.*, 2010).

The 2002 M 7.9 Denali earthquake ruptured portions of the Central Denali fault before propagating southeastward along the Totschunda fault, instead of continuing along the Eastern Denali fault (Eberhart-Phillips *et al.*, 2003). Paleoseismic investigations along the Eastern Denali fault suggest multiple large (M >6) earthquakes have occurred over the last several thousand years (Blais-Stevens *et al.*, 2020). Furthermore, records of the largest dextral motion along the Denali fault are from the eastern segments (Lowey, 1998; Haeussler *et al.*, 2008). This suggests that the Eastern Denali fault played an important role in terrane assembly through geologic history and may have experienced local deformation. Yet, the Eastern Denali fault is currently seismically quiescent, and recent studies have proposed that it serves as a regional stress boundary while active deformation occurs farther westward (*e.g.*, Choi *et al.*, 2021). This is further supported by the hypothesis of an unmapped 'connector fault' that links the Fairweather and Totschunda faults and transfers strain between them (Richter and Matson, 1971; Lahr and Plafker, 1980; Doser, 2014). This structural feature is required to explain spatial variations in the direction and deformation rate observed from GPS measurements (*e.g.*, Elliott and Freymueller, 2020). Lastly, geodynamic modelling (Jadamec *et al.*, 2013) suggests the Denali fault system is a major geological boundary spanning from the surface through the entire lithosphere, and is required to explain deformation in south-central Alaska (the Wrangell block).

## Seismicity

Understanding modern seismicity provides a valuable constraint on fault behaviour, crustal stress and regional plate tectonics. Yet, studies on seismicity in southwestern Yukon have historically been limited by the sparse seismic network coverage throughout the region (Fig. 1). This is a consequence of the inaccessibility of the terrain, which is largely at high elevation and covered by ice. In 2010, network coverage in southwestern Yukon improved from effectively no broadband stations to more than 10, which decreased the minimum magnitude of catalogue completeness (in certain regions) from ~3.0 to ~1.0 (Meighan *et al.*, 2013). Since 2016, station coverage throughout the region has further improved with the deployment of large campaign experiments such as the Earthscope Transportable Array deployment in

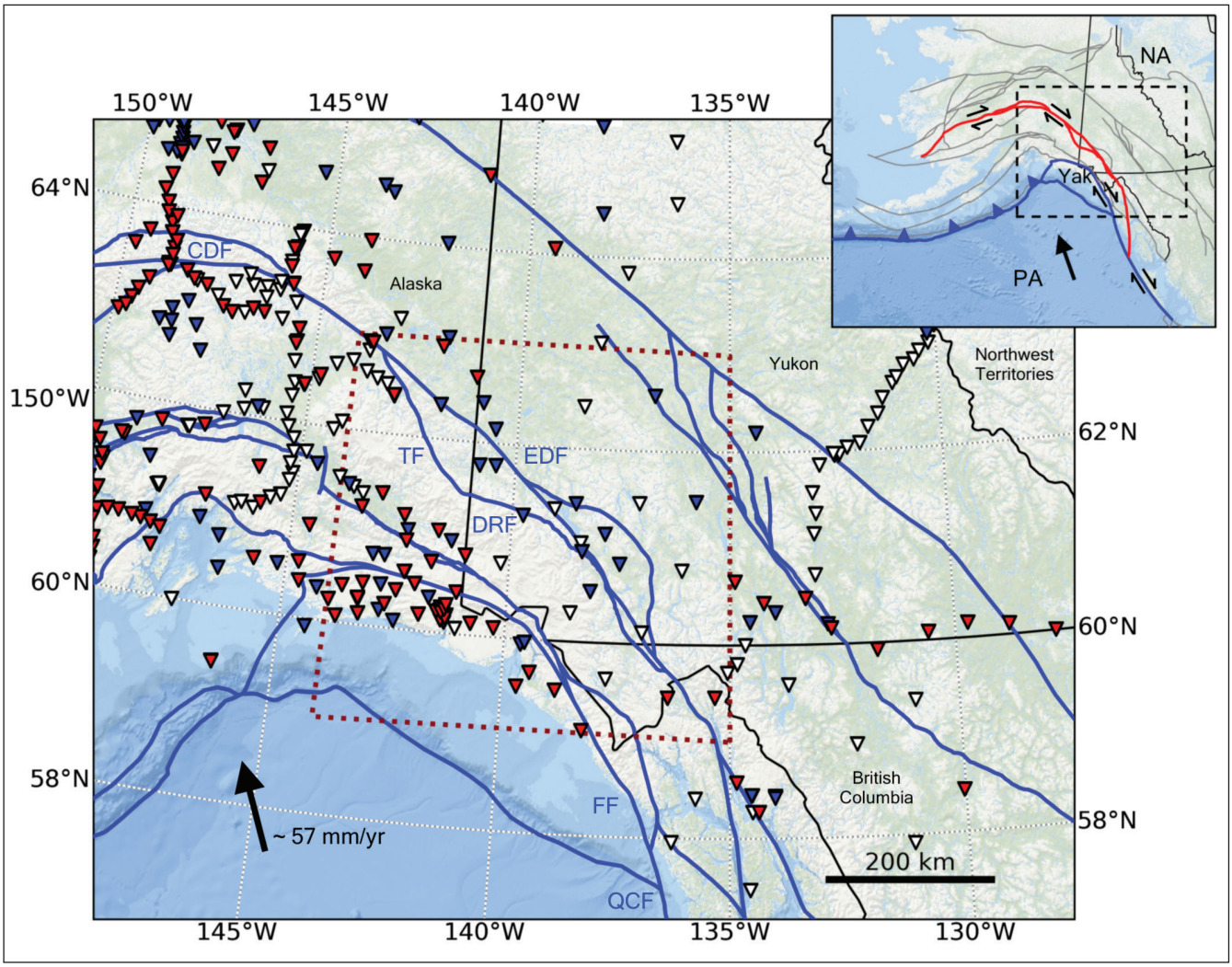


***Figure 1.*** *Regional tectonic setting and seismic station coverage. Permanent and temporary broadband seismic stations shown are coloured according to deployment date: prior to 2010 (red); between 2010 and 2016 (blue); and after 2016 (white). Note the relatively sparse broadband seismic station coverage in Yukon. Major faults are shown as blue lines (after Yukon Geological Survey, 2020). Faults discussed in the text are labelled: Central Denali fault (CDF); Eastern Denali fault (EDF); Totschunda fault (TF); Duke River fault (DRF); Fairweather fault (FF); Queen Charlotte fault (QCF). The red dashed box defines the study area shown in Figure 3. The inset map provides large-scale tectonic context of the interaction between the Pacific plate (PA), North American plate (NA), and Yakutat microplate (Yak). Plate boundaries are shown in blue. The Denali fault and associated faults discussed in the text are shown in red. Other major faults are shown in grey. Black arrow in both maps illustrates the plate vector and velocity of PA relative to NA (Kreemer et al., 2014).*

Alaska and western Yukon (Busby and Aderhold, 2020), and the Earthscope Mackenzie Mountains Transect (Baker et al., 2020). These further decreased the minimum magnitude of earthquake detection by 0.25–0.5 units in southwestern Yukon (Ruppert and West, 2020). These seismic station network improvements have also improved systematic earthquake location (horizontal) errors by up to tens of kilometres (Meighan et al., 2013).

Previous investigations on seismicity in this region have focused on local scales (e.g., Power, 1988), considered relatively large events recorded by distant stations (e.g., Horner, 1983; Doser, 2000, 2004; Doser and Rodriguez, 2011), or investigated nearby aftershock sequences (e.g., Doser, 2012). Seismological constraints on crustal stress necessitates analysis of earthquake source characteristics, including focal mechanisms and moment tensors. Such quantified stress estimates are

sparse in southwestern Yukon (Heidbach et *al*., 2018). Most studies on earthquake source characteristics in the region predate seismic station network improvements, and so generally only consider few of the largest events (*e.g*., Risteau et *al*., 2007; Kao et *al*., 2012; Doser, 2014). The global centroid moment tensor catalogue (Ekström et *al*., 2012) includes more than 30 events in southwestern Yukon (and surrounding regions) since 1980. The earthquake focal mechanism catalogue of the International Seismological Centre (ISC; Lentas et *al*., 2019) currently provides the most complete source characteristics catalogue, with over 123 events in the region since 2000. In general, seismicity throughout the region is dominated by reverse and dextral strike-slip faulting. In particular, seismicity is concentrated near the Duke River fault which exhibits mostly reverse faulting (*e.g*., Doser, 2014). The Central Denali fault and the northern extent of the Totschunda fault also exhibit abundant seismicity.

Improvements in seismic station network coverage over the last decade have significantly improved earthquake catalogues in southwestern Yukon. Yet, detailed seismological constraints on the crustal stress field throughout the region necessitate additional earthquake source mechanism estimates, with greater spatial coverage. In this report, we use P-wave first-motion polarities to probabilistically invert for focal mechanisms of small and moderate-magnitude earthquakes in southwestern Yukon and surrounding regions. We present an updated earthquake focal mechanism catalogue with 363 new events, and significantly improve spatial coverage. This work is part of a larger, multi-year study of natural hazards and geothermal resource potential in Yukon. The estimation of shallow Curie point depths (*e.g*., Li et *al*., 2017), the mapping of radiogenic rocks (*e.g*., Friend and Colpron, 2017; Colpron, 2019), and the presence of warm water springs (*e.g*., Langevin et *al*., 2020) suggest locations in Yukon may represent ideal targets for geothermal resources development. Results from this study will enable more detailed examination of the current behaviour of the Eastern Denali fault, and surrounding fault systems. This can be used to help assess natural hazards of the region as well as to estimate rock permeability near (and within) these systems, which is valuable for targeted geothermal exploration.

## Data and methods

For this study, we use earthquakes reported in the United States Geological Survey (USGS) catalogue as our study region spans part of southeastern Alaska. Specifically, we consider all events between 2016 and 2022 within our study region (dashed red box shown in Fig. 1) with $M \geq 3.0$ and depth $\leq 30$ km for focal mechanism estimation. Given the limited seismicity along the Eastern Denali fault, we extend our search criteria for candidate earthquakes to include all events within 50 km of the surface trace of the Eastern Denali fault between 2010 and 2022 with $M \geq 2.0$. For selected events, vertical-channel waveform data were retrieved for all seismic stations within 450 km epicentral distance. After applying a 1Hz high-pass filter, first-motion polarities (*i.e*., dilatational or compressional) were manually selected for stations with clear P-wave arrival onsets. Azimuth and takeoff angles were calculated using ray propagation through the standard velocity model used by the USGS for southeastern Alaska (Fogleman et *al*., 1993). Finally, polarities were inverted to estimate earthquake focal mechanisms within a Bayesian (probabilistic) framework using recent improvements (Hamidbeygi, 2022) to the Bayesian Earthquake Analysis Tools (BEAT) software (Vasyura-Bathke et *al*., 2020.

Understanding and quantifying the uncertainties in estimated earthquake focal mechanisms allows for more reliable interpretations of fault behaviour and, ultimately, regional tectonics. Bayesian inversion offers a means of rigorous model parameter uncertainty quantification, and its use in seismic source studies is established (see Vasyura-Bathke et *al*., 2020). Within a Bayesian inversion framework, model parameters and data are treated as random variables. The model parameters (strike, dip and rake of the focal mechanism) are constrained by data (P-wave polarities) as well as prior information. This can be informative (thereby providing additional constraint) or uninformative (allowing the solution to be predominantly constrained by data information). Specifically, Bayesian inversion updates the prior knowledge of the model parameters using data to determine the posterior probability density (PPD) of the model parameters, which represents the solution to the inverse problem (Jaynes, 2003).

These are related through Bayes' theorem, which is given by:

$$P(\boldsymbol{m}|\boldsymbol{d}) = \frac{P(\boldsymbol{m})P(\boldsymbol{d}|\boldsymbol{m})}{P(\boldsymbol{d})} \quad (1)$$

where $\boldsymbol{m}$ and $\boldsymbol{d}$ are vectors of model parameters and data, respectively. $P(\boldsymbol{m})$ is the prior probability density of the model parameters, independent of the data. In this study, priors are uniform distributions bounded by the physical limits of strike, dip and rake (*i.e.*, uninformative). $P(\boldsymbol{m} \mid \boldsymbol{d})$ is the conditional probability of the model parameters given the data, which is the PPD. Conversely, is the conditional probability of the data given the model parameters. In practice, once the data are measured/observed they represent a fixed realization of a random variable. In which case, this conditional probability represents the likelihood $L(\boldsymbol{m})$ that a set of model parameters can reproduce the observed data. $P(\boldsymbol{d})$ provides a normalization independent of the model parameters and is not required to be known for the purpose of this study (MacKay, 2003).

Assuming the data residuals (differences between observed and predicted data) to be a representation of data errors, a likelihood function can be formulated by assuming their statistical distribution (given the model). The likelihood function implemented in BEAT for the inversion of P-wave polarity data assigns higher probability to arrivals that have a greater theoretical amplitude, depending on their location on the focal sphere (Brillinger *et al.*, 1980). This is chosen as P-wave polarity data that are located near mechanism planes theoretically have smaller amplitudes and are likely to be less reliable due to potential modelling errors in azimuths and takeoff angles (due to inaccurate velocity models, event hypocentres, etc.). Furthermore, it stands to reason that higher amplitude P-wave arrivals provide more reliable (higher signal-to-noise ratio; SNR) waveforms for first-motion polarity assignment.

Specifically, this likelihood is the product of probabilities (for independent polarity data) given by:

$$L(\boldsymbol{m}) = \prod_{i=1}^{N} \pi_i^{\frac{(1+d_i)}{2}} (1-\pi_i)^{\frac{(1-d_i)}{2}} \quad (2)$$

where $d_i$ is the polarity datum at station *i*, and $\pi_i$ is given by:

$$\pi_i = \gamma + (1-2\gamma)\phi\left(\frac{A_i(\boldsymbol{m})}{\sigma}\right). \quad (3)$$

Here, $\phi(\cdot)$ is the cumulative distribution function of the normal distribution, which provides an estimate of polarity probability given a theoretical amplitude $A_i(\boldsymbol{m})$ and modelling error standard deviation $\sigma$ (where $\sigma > 0$). Lastly, defines the probability that the polarity has been assigned incorrectly $(0 \geq \gamma \geq 0.5)$, and can be considered small for high SNR data. In this work, we treat as a hyper-parameter that is estimated as part of the inversion. We define a uniform prior on $\sigma$, bounded between 0 and 0.2. This provides a flexible representation of data errors, which is solved for as part of the inversion. We assume a conservative probability of incorrect polarity assignment of 0.2 (value for $\gamma$) that enables additional flexibility in the error model.

In general, it is challenging (and sometimes impossible) to determine an analytical solution for the PPD (Equation 1). Instead, numerical methods are used to draw samples from the PPD. The ensemble of samples can then be used as an approximation of the PPD to estimate its properties. The inversion method implemented in BEAT, and used in this study, estimates the PPD via a sequential Monte Carlo sampler (Del Moral *et al.*, 2006). The samples are independent and based on a sequence of intermediate distributions (*i.e.*, stages) that transition between the prior and posterior, controlled by a scaling parameter. Depending on the choice of prior, this implementation allows for wide (unrestricted) initial exploration of the parameter space, which then becomes more constrained by the data (via the likelihood function) as the inversion progresses towards the posterior. All inversions in this work are run with 2000 sampling chains with 300 steps each. The number of sequential stages is adapted according the polarity data set for each inversion (typically <5);

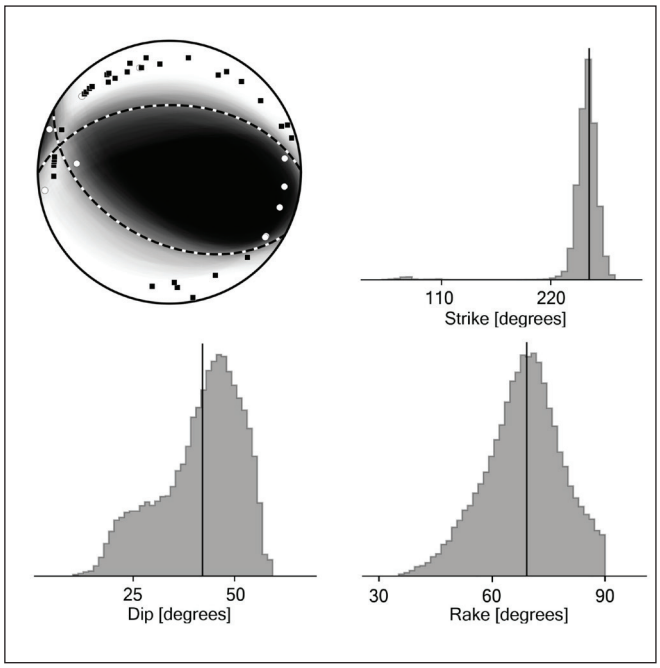


***Figure 2.*** *An example of Bayesian focal mechanism inversion from polarity data. Inversion results are shown for an M3.6 event that occurred on February 28, 2017. The 'fuzzy beachball' is shown for an ensemble of 200 focal mechanisms drawn from the posterior probability density (top left). White circle and black squares represent positive and negative polarity data, respectively, located at the modelled azimuth and take-off angles. The marginal posterior distributions are also shown for the strike, dip and rake of one of the mechanism planes. Vertical lines in the marginal distribution plots identify the location of the maximum probability model. The geographic location of this earthquake is shown in Figure 3.*

see Del Moral *et al.* (2006) and Vasyura-Bathke *et al.* (2020) for details. BEAT is a highly flexible program that can consider many additional parameters (*e.g.*, corrections to hypocentre locations), more complex source types, as well as other seismic and geodetic data types (*e.g.*, waveforms). Future research directions include comprehensive use of BEAT capabilities for data from southwestern Yukon, as well as improvements to BEAT for polarity data inversion.

Figure 2 shows an example of the results of Bayesian focal mechanism inversion of P-wave polarity data for an M 3.6 earthquake that occurred on February 28, 2017. A focal mechanism solution is typically represented graphically by a 'beachball' diagram that is a stereonet projection of the lower half of the focal sphere. The advantage of Bayesian inversion is rigorous uncertainty quantification. In this case, uncertainty in the focal mechanism solution is visually represented by a 'fuzzy beachball' diagram, which is estimated from samples drawn from the PPD (in this case 200 samples). If the diagram is a sharp image, it implies the PPD is more localized in the model parameter space (*i.e.*, smaller uncertainty). Figure 2 also shows the marginal posterior distributions for the individual focal mechanism parameters (strike, dip and rake of one of the mechanism planes), which reveal the uncertainty in these parameters. The geographic location of the earthquake used in this example is shown in Figure 3.

## Results and discussion

We performed Bayesian focal mechanism inversions for events with a minimum of 10 polarity observations. In total, we present focal mechanism inversion results for 363 events in southwestern Yukon and the surrounding region. Figure 3 summarizes our updated focal mechanism catalogue by showing the P-axis (pressure) trends for the maximum probability focal mechanism model from each inversion, coloured according to event faulting type (as defined by Kaverina *et al.*, 1996, and Álvarez-Gómez, 2019). It is well known that P-wave first-motion polarity data provide no information to constrain which of the two nodal planes in each focal mechanism is the actual fault plane. Furthermore, the P-axis of a focal mechanism is a geometrical property related to an individual earthquake, whereas the vector of principle crustal stress applies to a volume of rock, and can activate faults with a variety of geometries (McKenzie, 1969). Specifically, the principle stress vector lies within the pressure quadrant of an individual focal mechanism (McKenzie, 1969). Despite these limitations, examination of P-axis trends provides insight into the behaviour of regional seismicity and individual fault structures, as well as a first-order understanding of crustal stress.

Along the Eastern Denali fault (and Duke River fault), we observe relatively consistent southwest-trending P-axis orientations, with a slight rotation to a more south-southwest (or even south) orientation for events located farther toward the northwest, particularly along the western segment of the Duke River fault. Events to the southwest of the Fairweather fault system

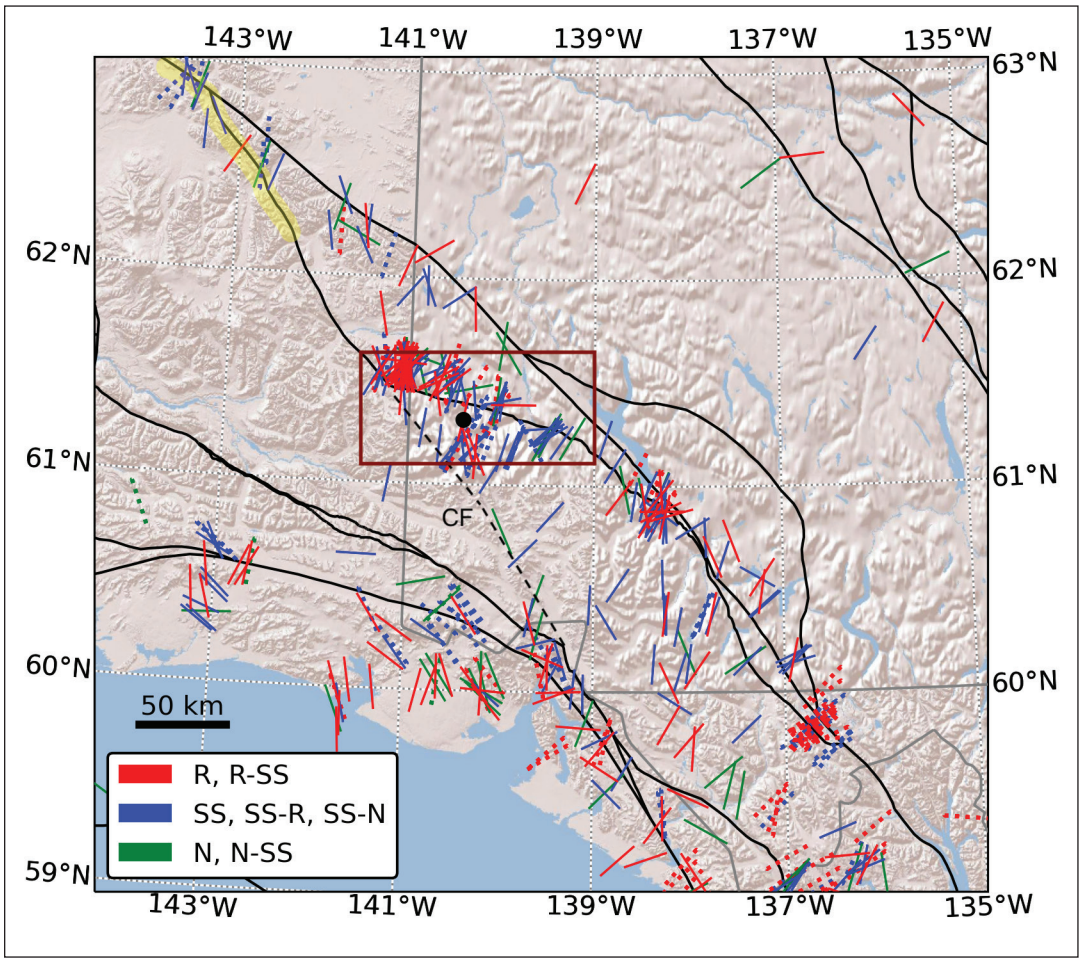


***Figure 3.*** *Updated earthquake focal mechanism catalogue for the SW Yukon. P-axis trends are shown for all focal mechanism estimates, coloured according to faulting mechanism classification (abbreviations for mechanism types as in Fig. 5). Dashed P-axis trends are from the ISC catalogue (between 2000 and 2022; Lentas et al., 2019). The location of the February 28, 2017 event (Fig. 2) is shown by the black circle. The boundary of the map shown in Figure 6 is delineated by the dark red box. The surface traces of major faults are shown as black lines (after Yukon Geological Survey, 2020). The dashed black line illustrates the postulated Connector fault (CF). The approximate rupture of the 2002 Denali earthquake is highlighted in yellow (after Eberhart-Phillips et al., 2003).*

exhibit P-axis orientations that are predominantly south-trending or rotated to southeasterly trends (Fig. 4), potentially indicating distinct stress orientations on either side of this fault system.

The ternary plot (Kaverina et al., 1996; Álvarez-Gómez, 2019) shown in Figure 5 indicates that our results consist mostly of a mixture of reverse and strike-slip faulting mechanisms. We also observe this general combination of faulting mechanisms spatially (Fig. 3), but note few, localized normal-faulting events. Furthermore, we note that the majority of the focal mechanism solutions are reported for events clustered near the Duke River fault, as well as an apparent (geologically) unmapped fault south of the Duke River fault. This focus region is highlighted in Figure 6. Specifically, we note that the Duke River fault exhibits predominantly reverse mechanisms with P-axes trending south-southwest, while the unmapped fault trace appears to be west-southwestward oriented and it exhibits predominantly strike-slip faulting with P-axes trending to the southwest. This is likely a continuation of a fault mapped at lower elevations to the northwest (e.g., Dodds and Campbell, 1992) that exhibit seismicity beneath the St. Elias icefields.

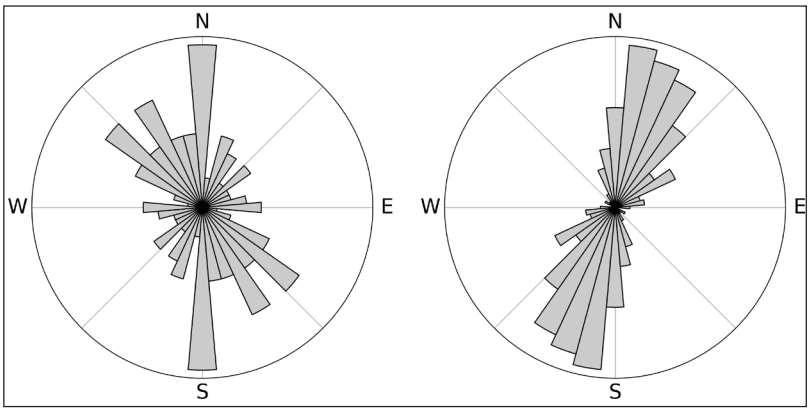


***Figure 4.*** *Regional P-axis trends from focal mechanisms estimated for events located southwest of the Fairweather fault system (left) and northeast of the Fairweather fault system (right).*

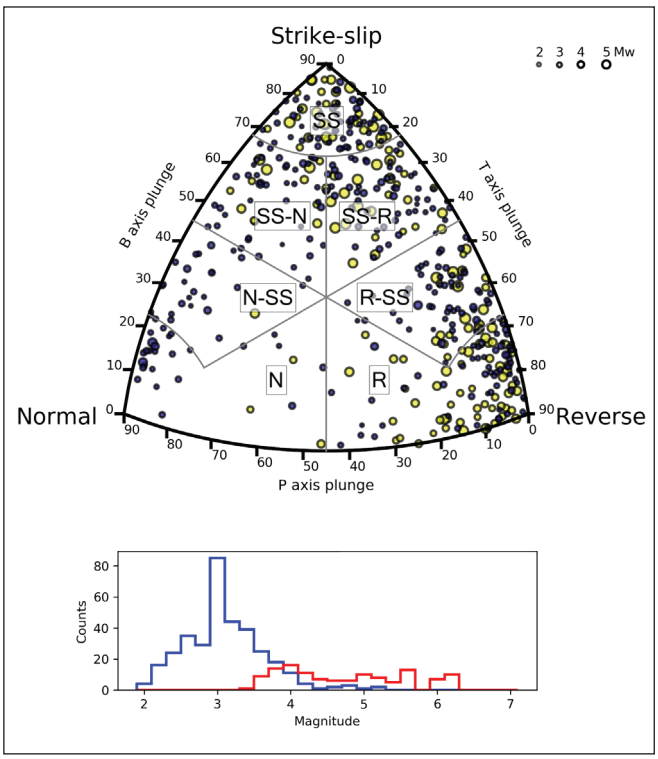


***Figure 5.*** *Focal mechanism distributions for southwestern Yukon. Earthquake faulting mechanism types are shown on the ternary diagram (top), with corresponding mechanism classification boundaries (Kaverina et al., 1996; Álvarez-Gómez, 2019). Dark blue and yellow circles represent focal mechanisms from this study and the ISC catalogue (between 2000 and 2022; Lentas et al., 2019), respectively. P and T axes refer to pressure and tension axes, respectively. The B axis is the intersection of the focal mechanism nodal planes, and is normal to the P and T axes. The distribution of earthquake magnitudes considered for focal mechanism estimation is shown (bottom) for the ISC catalogue (red) and this study (blue).*

Of note, Meighan et *al.* (2013) and Doser (2014) identified a band of seismicity south of the Duke River fault, which is likely the same unmapped feature discussed above. Seismicity also suggests the westernmost Duke River fault may be connected to this unmapped feature via a south-oriented fault; potentially the 'connector fault' that connects farther south with the Fairweather fault system. Limited focal mechanism estimates (Figs. 3 and 6) suggest consistent strike-slip faulting on this feature. Meighan et *al.* (2013) and Doser (2014) also identified a westward-oriented band of seismicity between the Totschunda fault and Eastern Denali fault, above 62° northern latitude (Fig. 3). Our results suggest a mixture of mostly strike-slip and reverse faulting here. Interestingly, this feature intersects the Totschunda fault near the rupture terminus of the 2002 Denali earthquake (Doser, 2014), suggesting a possible avenue for strain transfer that circumvents the southern Totschunda fault (Fig. 3).

Focal mechanism estimates from the ISC catalogue between 2000 and 2022, for our study region, are also shown in Figures 3, 5 and 6 (Lentas et *al.*, 2019). We note that this catalogue only consists of the largest events in the region over the last 2 decades. By comparison, the results presented in this work include focal mechanisms for smaller events over a shorter time period (of significantly improved seismic station spatial coverage), that has allowed us to improve the total focal mechanism catalogue for southwestern Yukon by approximately a factor of 4 (Fig. 5). We also note an improvement in focal mechanism spatial coverage throughout the region (Fig. 3). Lastly, the localized consistency between the results presented here and the ISC catalogue (Figs. 3 and 6) lend confidence in our analysis.

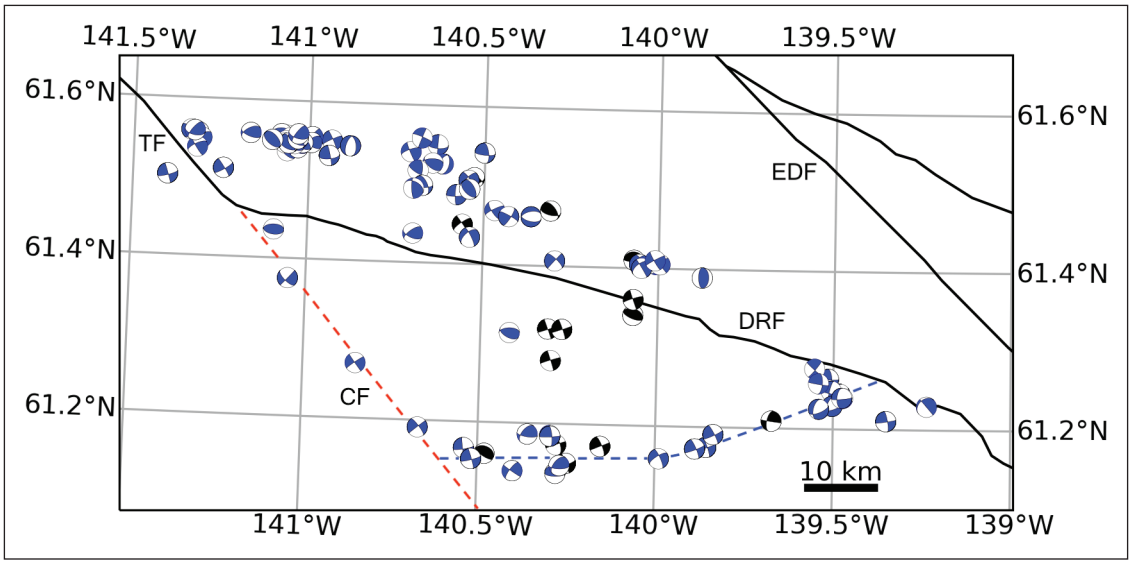


***Figure 6.*** *Earthquake focal mechanism solutions near the Duke River fault (DRF). Solutions from this study and the ISC catalogue (between 2000 and 2022; Lentas et al., 2019) are shown as blue and black beachball diagrams, respectively. The boundary of this map is shown in Figure 3. The surface traces of major faults are shown as black lines (after Yukon Geological Survey, 2020), including: the Totschunda fault (TF), the DRF, and the Eastern Denali fault (EDF). The red dashed line illustrates the postulated Connector fault (CF), and the blue dashed line illustrated the unmapped fault discussed in the text.*

A future research objective includes further refinement of the regional focal mechanism catalogue for southwestern Yukon. Specifically, we intend to use a relocated event catalogue (Biegel et *al.*, 2023) to update event hypocentres and more-accurately model azimuths and take-off angles. It has recently been demonstrated that centroid moment tensors for small earthquakes (~M 1.0) can be estimated via joint inversion of multiple seismic data types including P-wave first-motion polarities, amplitude spectra, and low-frequency waveforms (Hamidbeygi, 2022). We intend to augment our catalogue of earthquake source characteristics by analyzing smaller events in regions within southwestern Yukon where few events occur that are large enough for reliable focal mechanism estimation from polarity data alone. Furthermore, we have recently deployed seismic stations at several focus areas throughout southern Yukon with the aim of improving seismicity catalogues, including estimating event source characteristics, in order to help in the assessment of natural hazards and geothermal resource potential at these locations. Finally, we intend to use our estimated focal mechanism catalogue, with associated uncertainty, as input for the inversion of regional crustal stress (*e.g.*, Arnold and Townend, 2007; Herrera et *al.*, 2021). Stress analysis from individual geographical clusters of earthquakes will allow us to quantify how stress varies spatially through this complex tectonic environment.

## Conclusions

Southwestern Yukon is a region of complex active tectonics, with historically sparse seismic station coverage. We leverage recent improvements in station coverage over the last decade to estimate focal mechanisms for smaller earthquakes than those that are routinely considered throughout the region. We employ a Bayesian (probabilistic) inversion method to estimate focal mechanism parameters, and rigorously quantify uncertainty, for 363 events. Examination of the spatial variability of faulting types and orientations reveals consistent mechanism throughout the region, with the majority of events exhibiting reverse and strike-slip faulting. We observe a contrast in P-axis orientation for events northeast vs. southwest of the Fairweather fault system, potentially suggesting different stress regimes. Furthermore, we observe a rotation in P-axis orientations along strike of the Eastern Denali and Duke River fault systems. Our results provide additional constraints on the faulting behaviour of features previously identified from regional seismicity.

Our results are also consistent with previous studies of earthquake source characteristics in the region, and provide an improvement in overall constraint and spatial coverage that will enable more-detailed analysis of regional active tectonics. The results presented here represent a preliminary update to the regional focal mechanism catalogue. Future work will aim to further refine and augment this catalogue.

## Acknowledgements

This work is supported by the Natural Science and Engineering Research Council (Canada) through a Postdoctoral Fellowship to Jeremy M. Gosselin and a Discovery Grant to Jan Dettmer, and by the Yukon Geological Survey through funding from Natural Resources Canada's Emerging Renewal Power Program and the Yukon government's *Our Clean Future* initiative. We thank Kluane First Nation for their support of this research. All seismic data used in this work are freely available for download through the international Federation of Digital Seismograph Networks (FDSN) Web Services of the facilities of the Incorporated Research Institutions for Seismology (IRIS; https://service.iris.edu/). Data were downloaded and processed using ObsPy (Beyreuther *et al.*, 2010), and polarities were manually assigned using Pyrocko/Snuffler (Heimann *et al.*, 2017). We thank Carlos Herrera for useful early discussions on focal mechanism inversion, and Maurice Colpron for helpful comments that improved this manuscript. We thank Clément Estève for a constructive critical review of this work. Tabulated focal mechanism solutions are available (Appendix 1) for download alongside this manuscript.

## References

Álvarez-Gómez, J.A., 2019. FMC—Earthquake focal mechanisms data management, cluster and classification. SoftwareX, vol. 9, p. 299–307, https://doi.org/10.1016/j.softx.2019.03.008.

Arnold, R. and Townend, J., 2007. A Bayesian approach to estimating tectonic stress from seismological data. Geophysical Journal International, vol. 170, no. 3, p. 1336–1356, https://doi.org/10.1111/j.1365-246X.2007.03485.x.

Baker, M.G., Heath, D.C., Schutt, D.L., Aster, R.C., Cubley, J.F. and Freymueller, J.T., 2020. The Mackenzie Mountains EarthScope Project: Studying active deformation in the northern North American Cordillera from margin to craton. Seismological Research Letters, vol. 91, no. 1, p. 521–532, https://doi.org/10.1785/0220190139.

Beyreuther, M., Barsch, R., Krischer, L., Megies, T., Behr, Y. and Wassermann, J., 2010. ObsPy: A Python toolbox for seismology. Seismological Research Letters, vol. 81, p. 530–533, https://doi.org/10.1785/gssrl.81.3.530.

Biegel, K., Gosselin, J. and Dettmer, J., 2023. Preliminary double-difference relocation catalogue of southwestern Yukon centred along the Denali fault zone. *In:* Yukon Exploration and Geology 2022, K.E. MacFarlane (ed.), Yukon Geological Survey.

Bemis, S.P., Weldon, R.J. and Carver, G.A., 2015. Slip partitioning along a continuously curved fault: Quaternary geologic controls on Denali fault system slip partitioning, growth of the Alaska Range, and the tectonics of south-central Alaska. Lithosphere, vol. 7, p. 235–246, https://doi.org/10.1130/L352.1.

Blais-Stevens, A., Clague, J.J., Brahney, J., Lipovsky, P., Haeussler, P.J. and Menounos, B., 2020. Evidence for large Holocene earthquakes along the Denali fault in southwest Yukon, Canada. Environmental and Engineering Geoscience, vol. 26, p. 149–166, https://doi.org/10.2113/EEG-2263.

Brillinger, D.R., Udias, A. and Bolt, B.A., 1980. A probability model for regional focal mechanism solutions. Bulletin of the Seismological Society of America, vol. 70, p. 149–170, https://doi.org/10.1785/BSSA0700010149.

Busby, R.W. and Aderhold, K., 2020. The Alaska transportable array: As built. Seismological Research Letters, vol. 91, p. 3017–3027, https://doi.org/10.1785/0220200154.

Choi, M., Eaton, D.W. and Enkelmann, E., 2021. Is the Eastern Denali fault still active? Geology, vol. 49, p. 662–666, https://doi.org/10.1130/G48461.1.

Colpron, M., 2019. Potential radiogenic heat production from granitoid plutons in Yukon. Yukon Geological Survey, Open File 2019-16.

Del Moral, P., Doucet, A. and Jasra, A., 2006. Sequential monte carlo samplers. Journal of the Royal Statistical Society: Series B (Statistical Methodology), vol. 68, p. 411–436.

Dodds, C.J. and Campbell, R.B., 1992. Geology of SW Kluane Lake Map Area (115G and F (E 1/2)) southwestern Yukon (1:250 000 scale). Geological Survey of Canada, Open File 2188.

Doser, D.I., 2004. Seismicity of the Denali–Totschunda fault zone in central Alaska (1912–1988) and its relation to the 2002 Denali fault earthquake sequence. Bulletin of the Seismological Society of America, vol. 104, p. S132–S144, https://doi.org/10.1785/0120040611.

Doser, D.I., 2012. Revisiting the 1979 St. Elias, Alaska, aftershock sequence and its regional significance. Bulletin of the Seismological Society of America, vol. 102, p. 2392–2404, https://doi.org/10.1785/0120120007.

Doser, D.I., 2014. Seismicity of southwestern Yukon, Canada, and its relation to slip transfer between the Fairweather and Denali fault systems. Tectonophysics, vol. 611, p. 121–129, https://doi.org/10.1016/j.tecto.2013.11.018.

Doser, D.I. and Lomas, R., 2000. The transition from strike-slip to oblique subduction in south- eastern Alaska from seismological studies. Tectonophysics, vol. 316, p. 45–65, https://doi.org/10.1016/S0040-1951(99)00254-1.

Doser, D.I. and Rodriguez, H., 2011. A seismotectonic study of the southeastern Alaska region. Tectonophysics, vol. 497, p. 105–113, https://doi.org/10.1016/j.tecto.2010.10.019.

Eberhart-Phillips, D., Haeussler, P.J., Freymueller, J.T., Frankel, A.D., Rubin, C.M., Craw, P., ... and Wallace, W.K., 2003. The 2002 Denali fault earthquake, Alaska: A large magnitude, slip-partitioned event. Science, vol. 300, p. 1113–1118, https://doi.org/10.1126/science.1082703.

Ekström, G., Nettles, M. and Dziewoński, A.M., 2012. The global CMT project 2004–2010: Centroid-moment tensors for 13,017 earthquakes. Physics of the Earth and Planetary Interiors, vol. 200, p. 1–9, https://doi.org/10.1016/j.pepi.2012.04.002.

Elliott, J.L., Larsen, C.F., Freymueller, J.T. and Motyka, R.J., 2010. Tectonic block motion and glacial isostatic adjustment in southeast Alaska and adjacent Canada constrained by GPS measurements. Journal of Geophysical Research: Solid Earth, vol. 115, B09407, https://doi.org/10.1029/2009JB007139.

Elliott, J. and Freymueller, J.T., 2020. A block model of present-day kinematics of Alaska and western Canada. Journal of Geophysical Research: Solid Earth, vol. 125, e2019JB018378, https://doi.org/10.1029/2019JB018378.

Fogleman, K.A., Lahr, J.C., Stephens, C.D. and Page, R.A., 1993. Earthquake locations determined by the southern Alaska seismograph network for October 1971 through May 1989. US Geological Survey Open-File Report 93-309, 54 p.

Friend, M. and Colpron, M., 2017. Potential radiogenic heat production from Cretaceous and younger granitoid plutons in southern Yukon (1:1 000 000 scale). Yukon Geological Survey, Open File 2017-60, 1 map and data.

Grantz, A., 1966. Strike-slip faults in Alaska. US Geological Survey Open-File Report 66-53, 82 p.

Haeussler, P.J., 2008. An overview of the neotectonics of interior Alaska: Far-field deformation from the Yakutat microplate collision. *In:* Active Tectonics and Seismic Potential of Alaska, J.T. Freymueller, P.J. Haeussler, R.L. Wesson, and G. Ekström (eds), American Geophysical Union, Geophysical Monograph, vol 179, p. 83–108, https://doi.org/10.1029/179GM05.

Hamidbeygi, M., 2022. Nonlinear Bayesian estimation of centroid moment tensors using multiple seismic data sets in the Kiskatinaw seismic monitoring and mitigation area. Unpublished MSc thesis, University of Calgary, Alberta, Canada.

Heidbach, O., Rajabi, M., Cui, X., Fuchs, K., Müller, B., Reinecker, J., ... and Zoback, M., 2018. The World Stress Map database release 2016: Crustal stress pattern across scales. Tectonophysics, vol. 744, p. 484–498, https://doi.org/10.1016/j.tecto.2018.07.007.

Heimann, S., Kriegerowski, M., Isken, M., Cesca, S., Daout, S., Grigoli, F., Juretzek, C., Megies, T., Nooshiri, N., Steinberg, A., Sudhaus, H., Vasyura-Bathke, H., Willey, T. and Dahm, T., 2017. Pyrocko - An open-source seismology toolbox and library. GFZ Data Services. https://doi.org/10.5880/GFZ.2.1.2017.001.

Herrera, C., Cassidy, J.F., Dosso, S.E., Dettmer, J., Bloch, W., Sippl, C. and Salazar, P., 2021. The crustal stress field inferred from focal mechanisms in northern Chile. Geophysical Research Letters, vol. 48, e2021GL092889, https://doi.org/10.1029/2021GL092889.

Horner, R.B., 1983. Seismicity in the St. Elias, region of northwestern Canada and southeastern Alaska. Bulletin of the Seismological Society of America, vol. 73, p. 1117–1137, https://doi.org/10.1785/BSSA0730041117.

Jadamec, M.A., Billen, M.I. and Roeske, S.M., 2013. Three-dimensional numerical models of flat slab subduction and the Denali fault driving deformation in south-central Alaska. Earth and Planetary Science Letters, vol. 376, p. 29–42, https://doi.org/10.1016/j.epsl.2013.06.009.

Jaynes, E.T., 2003. Probability theory: The logic of science. Cambridge university press.

Kalbas, J.L., Freed, A.M., and Ridgway, K.D., 2008. Contemporary fault mechanics in southern Alaska. *In:* Active Tectonics and Seismic Potential of Alaska, J.T. Freymueller, P.J. Haeussler, R.L. Wesson, and G. Ekström (eds), American Geophysical Union, Geophysical Monograph Series 179, p. 321–336.

Kaverina, A.N., Lander, A.V. and Prozorov, A.G., 1996. Global creepex distribution and its relation to earthquake-source geometry and tectonic origin. Geophysical Journal International, vol. 125, p. 249–265, https://doi.org/10.1111/j.1365-246X.1996.tb06549.x.

Kao, H., Shan, S.J., Bent, A., Woodgold, C., Rogers, G., Cassidy, J.F. and Ristau, J., 2012. Regional centroid-moment-tensor analysis for earthquakes in Canada and adjacent regions: An update. Seismological Research Letters, vol. 83, p. 505–515, https://doi.org/10.1785/gssrl.83.3.505.

Kreemer, C., Blewitt, G. and Klein, E.C., 2014. A geodetic plate motion and Global Strain Rate Model. Geochemistry, Geophysics, Geosystems, vol. 15, p. 3849–3889, https://doi.org/10.1002/2014GC005407.

Lahr, J.C. and Plafker, G., 1980. Holocene Pacific-North America plate interaction in southern Alaska: implications for the Yakataga seismic gap. Geology, vol. 8, p. 483–486, https://doi.org/10.1130/0091-7613(1980)8<483:HPAPII>2.0.CO;2.

Langevin, H., Raymond, J. and Fraser, T., 2020. Assessment of thermo-hydraulic properties of rock samples near Takhini Hot Springs, Yukon. *In:* Yukon Exploration and Geology 2019, K.E. MacFarlane (ed.), Yukon Geological Survey, p. 57–73.

Lentas, K., Di Giacomo, D., Harris, J. and Storchak, D.A., 2019. The ISC Bulletin as a comprehensive source of earthquake source mechanisms. Earth System Science Data, vol. 11, p. 565–578, https://doi.org/10.5194/essd-11-565-2019.

Leonard, L.J., Hyndman, R.D., Mazzotti, S., Nykolaishen, L., Schmidt, M. and Hippchen, S., 2007. Current deformation in the northern Canadian Cordillera inferred from GPS measurements. Journal of Geophysical Research: Solid Earth, vol. 112, B11401, https://doi.org/10.1029/2007JB005061.

Leonard, L.J., Mazzotti, S. and Hyndman, R.D., 2008. Deformation rates estimated from earthquakes in the northern Cordillera of Canada and eastern Alaska. Journal of Geophysical Research: Solid Earth, vol. 113, B08406, https://doi.org/10.1029/2007JB005456.

Li, C.F., Lu, Y. and Wang, J., 2017. A global reference model of Curie-point depths based on EMAG2. Scientific reports, vol. 7, p. 1–9, https://doi.org/10.1038/srep45129.

Lowey, G.W., 1998. A new estimate of the amount of displacement on the Denali fault system based on the occurrence of carbonate megaboulders in the Dezadeash Formation (Jura-Cretaceous), Yukon, and the Nutzotin Mountains sequence (Jura-Cretaceous), Alaska. Bulletin of Canadian Petroleum Geology, vol. 46, p. 379–386, https://doi.org/10.35767/gscpgbull.46.3.379.

MacKay, D.J., 2003. Information theory, inference and learning algorithms. Cambridge university press.

Matmon, A., Schwartz, D P., Haeussler, P.J., Finkel, R., Lienkaemper, J.J., Stenner, H.D. and Dawson, T.E., 2006. Denali fault slip rates and Holocene–late Pleistocene kinematics of central Alaska. Geology, vol. 34, p. 645–648, https://doi.org/10.1130/G22361.1.

Marechal, A., Mazzotti, S., Elliott, J.L., Freymueller, J.T. and Schmidt, M., 2015. Indentor-corner tectonics in the Yakutat-St. Elias collision constrained by GPS. Journal of Geophysical Research: Solid Earth, vol. 120, p. 3897–3908, https://doi.org/10.1002/2014JB011842.

Marechal, A., Ritz, J.F., Ferry, M., Mazzotti, S., Blard, P.H., Braucher, R. and Saint-Carlier, D., 2018. Active tectonics around the Yakutat indentor: New geomorphological constraints on the eastern Denali, Totschunda and Duke River Faults. Earth and Planetary Science Letters, vol. 482, p. 71–80, https://doi.org/10.1016/j.epsl.2017.10.051.

McKenzie, D.P., 1969. The relation between fault plane solutions for earthquakes and the directions of the principal stresses. Bulletin of the Seismological Society of America, vol. 59, p. 591–601, https://doi.org/10.1785/BSSA0590020591.

Meighan, L.N., Cassidy, J.F., Mazzotti, S. and Pavlis, G.L., 2013. Microseismicity and tectonics of southwest Yukon Territory, Canada, using a local dense seismic array. Bulletin of the Seismological Society of America, vol. 103, p. 3341–3346, https://doi.org/10.1785/0120130068.

Nelson, J., Colpron, M. and Israel, S., 2013. The cordillera of British Columbia, Yukon, and Alaska: tectonics and metallogeny. *In:* Tectonics, Metallogeny, and Discovery: The North American Cordillera and Similar Accretionary Settings. Colpron, M., Bissig, T., Rusk, B.G., and Thompson, J.F.H., Society of Economic Geologists Special Publication, vol. 17, p. 53–109.

Power, M., 1988. Microearthquake seismicity on the Duke River, Denali Fault system. In: Yukon Geology, vol. 2, Exploration and Geological Services Division, Yukon, Indian and Northern Affairs Canada, p. 61–68.

Richter, D.H. and Matson, N.A., 1971. Quaternary faulting in the eastern Alaska Range. Geological Society of America Bulletin, vol. 82, p. 1529–1540.

Ristau, J., Rogers, G.C. and Cassidy, J.F., 2007. Stress in western Canada from regional moment tensor analysis. Canadian Journal of Earth Sciences, vol. 44, p. 127–148, https://doi.org/10.1139/e06-057.

Ruppert, N.A. and West, M.E., 2020. The impact of USArray on earthquake monitoring in Alaska. Seismological Research Letters, vol. 91, p. 601–610, https://doi.org/10.1785/0220190227.

Vasyura-Bathke, H., Dettmer, J., Steinberg, A., Heimann, S., Isken, M.P., Zielke, O., ... and Jónsson, S., 2020. The Bayesian earthquake analysis tool. Seismological Research Letters, vol. 91, p. 1003–1018, https://doi.org/10.1785/0220190075.

Waldien, T.S., Roeske, S.M., and Benowitz, J.A., 2021. Tectonic underplating and dismemberment of the Maclaren-Kluane Schist records Late Cretaceous terrane accretion polarity and ~480 km of post-52 Ma dextral displacement on the Denali fault. Tectonics, vol. 40, e2020TC006677, https://doi.org/10.1029/2020TC006677.

Yukon Geological Survey, 2020. A digital atlas of terranes for the northern Cordillera. Yukon Geological Survey, http://data.geology.gov.yk.ca/Compilation/2, [accessed, November, 2022].

## Appendix

The appendix is only available as a digital file (csv). It is included in a .zip file and accompanies this document; download from https://data.geology.gov.yk.ca.

Appendix 1 – Tabulated focal mechanism solutions